Time-resolved triggering and runout analysis of rainfall-induced shallow landslides

Noname manuscript No.
(will be inserted by the editor)

Time-resolved triggering and runout analysis of rainfall-induced shallow landslides

G. La Porta · A. Leonardi · M. Pirulli · F. Cafaro · F. Castelli

Received: date / Accepted: date

Abstract Rainfall-induced shallow landslides often turn into flows. These phenomena pose severe hazard to infrastructure and human lives on mountainous areas. Risk assessment, and the design of mitigation measures, can both be informed by back analysis of previous events. However, shallow instabilities are frequently spread over a large area, with the generated flows occurring in sequences, or surges. Conventionally, back-analysis exercises tackle the problem by simulating runout as a single event, with all surges happening simultaneously. This simplification has repercussions that have not been explored in the literature so far. Therefore, a novel time-resolving procedure is proposed in this paper, which can be applied to resolve instability sequences of arbitrary duration. The methodology discretizes the event, detecting instabilities at equally-spaced time intervals as a function of rainfall. Thanks to this, the post-failure behaviour of each surge can be tracked by a runout model, with a separate simulation performed every time a new instability is detected. The methodology is tested on two documented study cases. The results reveal that, under some conditions, the time-resolving procedure can lead to significantly different results in terms of runout path, flooded area, and flow heights. This has profound repercussions on how back-analysis is conventionally applied.

Keywords Flow-like landslides, rainfall-induced shallow landslides, landslide triggering and runout, landslide susceptibility, numerical modelling.

G. La Porta, M. Pirulli, F. Cafaro
Politecnico di Torino, Department of Structural, Geotechnical and Building Engineering, Corso Duca degli Abruzzi, 24, 10129, Torino, Italy
E-mail: giulia.laporta@polito.it

A. Leonardi
University of Sheffield, Department of Civil and Structural Engineering, Mappin Street, S1 3JD, Sheffield, UK

F. Castelli
Università degli Studi di Enna ”Kore”, Faculty of Engineering and Architecture, Cittadella Universitaria, 94100, Enna, Italy

1 Introduction

Flow-like landslides [26] represent a substantial hazard for human and structures, since they are characterized by long runout and high destructive power. One of their most important triggering factors is represented by rainfall, which can infiltrates slopes, leading to the mobilization of shallow soil deposits. According to Hutchinson [27], and Cruden and Varnes [15], rainfall-induced shallow landslide, in their initial stage after triggering, can be classified as translational slides. In the subsequent runout stage, they are often referred to as either flowslides, if undergoing static liquefaction, or as slides turning into flows [26] when seen as the cascading effect of local failures [16]. When fully mobilized as flows, they are often referred to as debris flows or mudflows, depending on whether the solid content is predominantly coarse- or fine-grained. In this stage, they tend to evolve into very rapid to extremely rapid phenomena (up to 20 m/s), with run-out distances that are up to two orders of magnitude higher than the length of the landslide source [9].

The ongoing changes in rainfall patterns are leading to a rise in the frequency of shallow landslide events involving long-runout mass flows. Furthermore, a growing urbanization of mountainous terrains is increasing risk on the global scale [36,6]. Among the different strategies for mitigating hazard, structural countermeasures such as barriers, check dams, and deflectors are often employed. The design of these structures can be supported by computational models. However, due to the extreme variability of site conditions, parameter calibration needs to be performed on each specific site. Alternatively, parameters can also be estimated from back-analysis of events on similar sites.

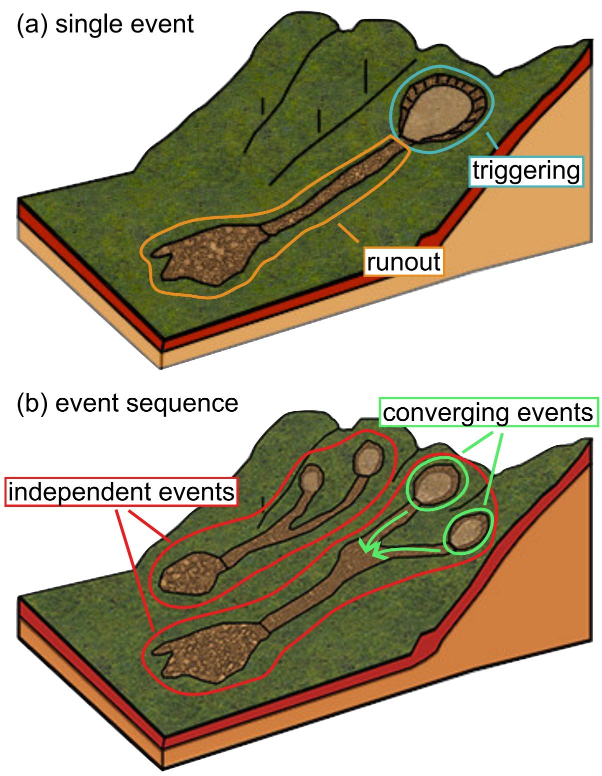

Fig. 1 Conceptual subdivision of (a) a single event into triggering and runout areas; (b) an event sequence in independent events on separate basins, and converging events within the same basin.

The back analysis of shallow landslides can be decomposed into two aspects, visually illustrated on **Fig. 1(a)**: (i) the *triggering problem*, i.e. the determination of the probability of failure and the event magnitude, and (ii) the *runout problem*: the estimation of the post-failure characteristics, such as flow volume, velocity, and composition. The *triggering problem* can be approached through either geomorphological-based [23], landslides inventories-based [63], heuristic [24], statistical, or process-based methods [49]. Among them, process-based and statistical methods are considered more advanced, being strictly quantitative. Statistical models are based on the analysis of instability factors (e.g., susceptible soil thickness and presence of vegetation), and on landslide inventories for instability mapping [62]. Process-based models employ limit equilibrium methods, or more complex finite-element approaches, to calculate a safety factor, interpreted as a measure of the susceptibility to failure [2].

The *runout problem* includes both flow propagation and deposition. The goal is to track the time evolution of variables such as flow depth, velocity and composition. Notably, the two-phase nature of fluidized soils can be modelled under either discrete or continuum assumptions. Discrete methods use assemblies of discrete Lagrangian particles to model the flow [59,54]. However, the number of particles that can be simulated is limited by computational resources. Continuum-based models tend therefore to be more efficient, and have been proposed in the literature in depth-averaged [52,47], three-dimensional [32,42], and coupled [40] frameworks. In depth-averaged models, the mass and momentum conservation equations are depth-averaged in the vertical direction. This approach can rely nowadays on a wide literature of applications on study cases [44,48]. It is therefore established as efficient and reliable. Nevertheless, limitations are present in the simulation of flow-structure interaction, where the three-dimensionality of the problem cannot be neglected.

Flows that generate from shallow landslides often occur in surges, i.e. multiple releases, converging on the same area. Surging is a multi-faceted behaviour, and can spontaneously arise from the rheological properties. Surges, or sequences, can also occur when slope failures are distributed on multiple source areas, as illustrated on **Fig. 1(b)**. This commonly happens when the triggering factor (a rainfall or a seismic event) causes instability on a regional or sub-regional scale. Examples of this are the events registered in the Clear Creek and Summit counties (Colorado, USA) in 1999, where 480 debris flows were triggered by a rainstorm in an area of 240 km^2 [22]. In 2008, almost 4000 shallow landslides were caused in Japan by an earthquake, registering around 23 fatalities and 450 injured [65]. A more recent event of this type is the sequence of post-wildfire debris flows triggered in Montecito (California, USA), which caused 23 casualties, and widespread disruption [4].

In these cases, there is an intrinsic uncertainty on whether the flows that are part of the same sequence can be back-analysed as mutually independent events. In the literature, events that occur within different basins, and whose runout do not converge (**Fig. 1(b)**), are usually analysed separately [4]. Within the same basin, flows with overlapping runout areas are treated as a single overarching event [33,34,31]. The latter is an approach where triggering is idealized as occurring at the same instant across the whole basin, with runout that develops from that time onward. Examples of back-analyses performed with this approach can be found in Cascini *et al.* [8], Stancanelli *et al.* [57], Chen *et al.* [12], and Tan *et al.* [60]. This inherently simplifies the time-evolution of the sequence. In particular, it implies that materials originating at the same distance from the fan apex generate flows that merge on the floodplain, regardless of whether this would have happened in the real event. This is problematic for two reasons: firstly, the flow generated from converging surges would have a significantly overestimated flow volume, height and momentum. Secondly, a back-analysis carried out without considering the actual time-sequence of the flows might yield calibrated material parameters that are biased.

To the authors' knowledge, the consequences of performing a back-analysis without resolving in time the flow sequence have not been discussed in the literature so far. This is likely due to the complex nature of the problem. Thus, to clarify these aspects, a numerical procedure for capturing the time evolution of shallow landslides, and subsequent flows within a basin, is proposed in this paper. The procedure is developed for rainfall-induced instabilities, and is based on well-established models for triggering and runout. The models are applied in a staggered fashion, employing a novel time-resolving algorithm. With it, instabilities and flow sequences within a basin can be detected and simulated with a prescribed time resolution, rather than as a single overarching event. The method is applied to two study cases, selected from within the same geographical area. The primary goal of this study is to understand whether a finer resolution in time leads to simulations that produce significantly different results. A secondary goal is to explore the role played by the input data resolution on the emergence of time-dependent effects.

The paper is organized as follows: Sec. 2 describes the proposed numerical procedure, which is then applied in Sec. 3 on a simple benchmark geometry. Sec. 4 is devoted to the description of the characteristics of the two case studies on which the methodology has been applied: the Sarno event [10], and the Giampilieri event [19]. Finally, Sec. 5 explores the applicability of the proposed framework. Implications on the back-analysis of events with a marked time-dependence are further discussed.

2 Description of the methodology

Table 1 Phases of the proposed methodology. t_i is the generic time interval i, between 1 and N, I_i is the hyetograph, V_i is the mobilized volume at the considered time, and the subscript f refers to the final configuration, after runout.

	Triggering		**Runout**	
	In	**Out**	**In**	**Out**
t_1	I_1	V_1	V_1	$V_{1,\mathrm{f}}$
t_2	$I_1 + I_2$	V_2	$V_2 + V_{1,\mathrm{f}}$	$V_{2,\mathrm{f}}$
t_3	$I_1 + I_2 + I_3$	V_3	$V_3 + V_{2,\mathrm{f}}$	$V_{3,\mathrm{f}}$
...	...	...	...	...
t_N	$\sum_{i=1}^{N} I_i$	V_N	$V_N + V_{N-1,\mathrm{f}}$	$V_{N,\mathrm{f}}$

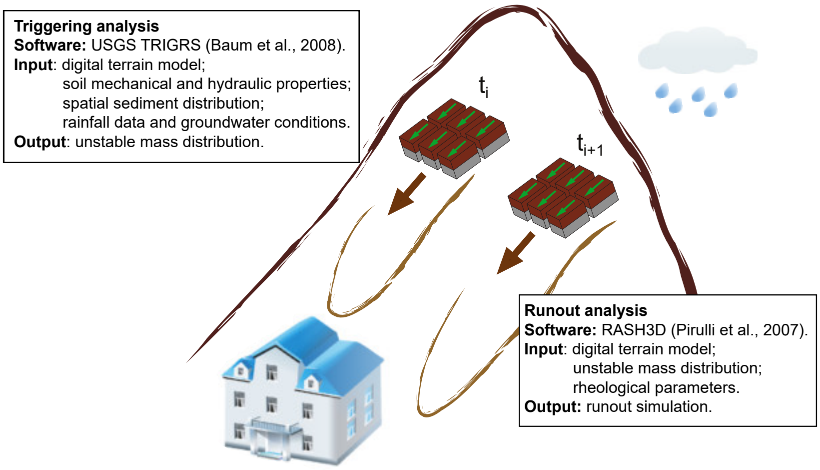

Fig. 2 Simulation procedure, with the conceptual separation into the triggering and the runout steps. The generic time intervals t_i and t_{i+1} refer to two consecutive triggering detection intervals i and $i+1$. Input and output parameters refer to the specific pieces of software employed for the analysis.

The outline of a generic time-resolved procedure is described in **Fig. 2**, which shows the required input data and the simulation output of both the triggering and the runout analyses. The figure illustrates how intense rainfall can induce, over time, a distribution of shallow instabilities on a slope. In addition to geomorphological data, the triggering analysis requires a hyetograph, i.e a resolution of the rainfall event as a sequence of mean rainfall intensities over specific time intervals (e.g. hourly). The sequence of instabilities is then computed as a function of the hyetograph, and is itself a function of time. Between two consecutive triggering analysis steps, a runout analysis is performed, tracking the propagation and deposition of the surges mobilized up to that point.

In **Table 1**, the proposed methodology is described in more details. The goal is to discretize the evolution of unstable, mobilized volumes V over time and space. Herein, the process is discretized into N equally-spaced time intervals [t_i - t_{i-1}], with $(i = 1, N)$. The triggering model identifies the distribution of volumes V_i that have become unstable during each time interval i. The triggering detection is based on a stress balance, which takes into account the groundwater conditions. Therefore, the unstable volume V_i is a function of the cumulative rainfall from the rainfall event start, up to t_i.

After each triggering step, the runout model tracks the propagation of the unstable volume detected by the triggering analysis, and determines the distribution of the volume at deposition $V_{i,\mathrm{f}}$. Note that during the runout step, the unstable volume is considered fully mobilized. Therefore, the time-evolution of pore pressure dissipation, and the strength degradation due to the loss of fabric are idealized as occurring instantaneously. This is a clear limitation of the procedure, which is however consistent with standard runout simulation practice. Consequently, the strength parameters during runout are lower than those used in the triggering analysis [1]. Each runout step propagates a distribution of volumes which is the juxtaposition of two contributions. The first one is the distribution of the newly mobilized volumes V_i, which is an output of the triggering analysis over the interval $t_i - t_{i-1}$. The second one is the distribution of the volumes deposited during the previous runout steps $V_{i-1,\mathrm{f}}$. This accounts for the possibility that previously deposited volumes might re-mobilize due to a new influx of material, a phenomenon often observed during surging [29].

The next sections will describe the mathematical and physical background of the triggering and propagation steps, and briefly describe the employed software.

2.1 Triggering analysis

The triggering analysis is performed under the hypothesis that instability is induced by rainfall, and that the rainfall event is uniform across the target area. Rainfall data is provided through a hyetograph, i.e. in terms of average intensity (e.g. mm/h), with a constant time interval (e.g., one hour). This choice is motivated by simplicity: indeed, non-constant time intervals could also be used. This would come with the potential benefit of a better representation of rainfall variations, especially peaks, but it would however imply a heavier computational load. Since rainfall data is already subject to a space approximation - monitoring stations are typically not within the landslide area - the simplification of a uniform time interval is considered adequate.

To compute stability, the limit equilibrium method is adopted, through a simplified analytical tool. The elevation model of the target area is divided into equally-spaced surface units, or cells. A key hypothesis is that stability can be evaluated for each cell independently. The software used is TRIGRS (Transient Rainfall Infiltration and Grid-Based Regional Slope-Stability Model, see Baum *et al.* [5]). The tool has been widely used and validated in the literature. Examples are the work of Salciarini *et al.* [51], who analysed the landslide susceptibility of an area of Umbria region, Italy, and of Park *et al.* [39], who compared the TRIGRS model results and observed instabilities from inventories of a region in Seoul, South Korea. Furthermore, Marin and Velásquez [35] verified the slope stability of an area in Valle de Aburrá (Colombia), studying the influence of hydraulic properties and conditions on shallow sliding failure susceptibility.

Starting from the digital elevation model, the rainfall data, and the morphological and lithological characteristics of the site, the program provides a space- and time-distribution of instabilities. This comes through the definition of a safety factor F_{S} on each cell. During a specific time interval, the factor of safety is computed as Taylor [61]:

$$F_{\mathrm{S},i}(z) = \frac{\tan\phi'}{\tan\delta} + \frac{c' - \Psi_i(z)\gamma_{\mathrm{w}}\tan\phi'}{\gamma_{\mathrm{s}} z \sin\delta}, \tag{1}$$

with ϕ' the effective friction angle, δ the cell slope angle, c' the effective cohesion, γ_{w} the unit weight of groundwater and γ_{s} the bulk unit weight. The coordinate z is the direction orthogonal to the topographical surface (the bed).

The hypothesis of tension-saturated initial conditions is adopted, and the impermeable basal boundary is fixed at a finite depth d_{l}. A physical limitation applied to the model is that the infiltration cannot overcome the saturated hydraulic conductivity k.

Under these hypotheses, the time-evolution of the groundwater pressure head $\Psi(t)$ from saturated initial conditions, is calculated as a function of the hyetograph $I(t)$ [5]. The tool considers infiltration, runoff, and flow routing. Therefore, on each cell, information on permeability k and on the saturated hydraulic diffusivity D is required. In agreement with Iverson [28], a physical upper limit is imposed to the pressure head, when the water table reaches the ground surface:

$$\Psi_i(z) \leq z \cos\delta, \tag{2}$$

In Eq. 1, a factor of safety less than or equal to 1 indicates instability. The value of z corresponding to $F_{\mathrm{S},i} = 1$ is the depth of unstable soil h. From this value, the unstable volume V can be computed by multiplying h by the cell area.

2.2 Runout analysis

Runout is modelled based on a continuum mechanics approach, using the numerical software RASH3D [46]. In the version used here, the software considers the unstable volume identified in the triggering step as a fully fluidized medium: an equivalent one-phase incompressible fluid with bulk mass density ρ_s. The software solves the depth-averaged balance equations in the hypothesis of isotropic distribution of normal stresses and absence of bed erosion:

$$\begin{cases} \dfrac{\partial h}{\partial t} + \dfrac{\partial(v_x h)}{\partial x} + \dfrac{(v_y h)}{\partial y} = 0 \\ h(\dfrac{\partial v_x}{\partial t} + v_x \dfrac{\partial v_x}{\partial x} + v_y \dfrac{\partial v_x}{\partial y}) = \\ \qquad \dfrac{1}{2}\dfrac{\partial(g_z h^2)}{\partial x} = \dfrac{1}{\rho_\mathrm{s}}\tau_{zx} + g_x h \\ h(\dfrac{\partial v_y}{\partial t} + v_x \dfrac{\partial v_y}{\partial x} + v_y \dfrac{\partial v_y}{\partial y}) = \\ \qquad \dfrac{1}{2}\dfrac{\partial(g_z h^2)}{\partial y} = \dfrac{1}{\rho_\mathrm{s}}\tau_{zy} + g_y h. \end{cases} \tag{3}$$

The software yields a time evolution of flow height h and velocity v over the target area. The bed shear stress, τ_z, describes the basal shear resistance between the flow and the sliding surface. Its definition requires the introduction of a rheological constitutive law. RASH3D contains multiple options for this term. Here, a Bingham rheology is employed, due to the predominantly fine nature of the solid fraction of both study cases [45]. The Bingham rheology, despite its simplicity, is very accurate in describing the runout of fine-grained shallow landslides undergoing mobilization [41]. Notably, a frictional law (e.g. Voellmy, consisting of a frictional and a velocity-dependent term, as in Ng *et al.* [37]) could also be adopted for coarser materials.

The Bingham rheology consists of a yield stress, below which the mass does not flow, and of a viscous term, which governs the post-yield behaviour. The depth-averaged version of the rheological constitutive equation is:

$$\tau_z^3 + 3(\frac{\tau_0}{2} + \frac{\eta_B v}{h})\tau_z^2 - \frac{\tau_0^3}{2} = 0. \quad (4)$$

In the relation, τ_0 is the yield stress, and η_B the Bingham viscosity.

To limit the complexity of the model, no erosion is considered in the proposed simulations. However, erosion could alter the flow kinematics, especially in rainfall events where saturation has weakened the bed material [48]. The entrainment of material along the flow path can alter the landslide soil characteristics, and increases the volume. Therefore, it can lead to important differences in terms of flow path and velocity. The choice to neglect the erosion could have effects on the back-analysis, providing under-estimated triggering parameters. However, as the main goal of the article is to isolate time-dependent effects, its addiction is not necessary here.

3 Benchmarking

Before approaching more complex study cases, a simplified scenario is simulated, as illustrated on **Fig. 3**. The goal is to verify weather, even on a very simple geometry, resolving instabilities in time can lead to significant changes in the back-analysis of an event.

The benchmark geometry is composed of a slope, representative of an idealized basin, which narrows in proximity of the fan apex. At the toe, a flat floodplain extends in all directions. The slope is divided into four sections with varying inclination: 25°, 22°, 20° and 18°, as shown in **Fig. 3a** with labels 1-4, respectively. The depth of mobilizable soil is also variable: 1, 1.5, 2 and 2.5 m, respectively. The slope and the floodplain are discretized with a uniform grid with 10×10 m spacing. The same spacing is used for the triggering and the runout simulations.

For the sake of simplicity, a constant-intensity rainfall event with $I = 35$ mm/h, representative of a severe rainstorm, is used to trigger instability. The geometry and the material are chosen so that the slope is everywhere close to limit equilibrium, and therefore susceptible to instability. Slope section 1 has an inclination and a depth of mobilizable soil that, in saturated conditions, yields a factor of safety of $F_S = 1.02$, calculated through TRIGRS. Sections $2-3-4$ are increasingly more stable ($F_S = 1.03$, 1.08, and 1.16, respectively). Therefore, it can be expected that the instabilities will initiate in the lower sections, and then progressively reach the uppermost sections. This choice is deliberate: in this way, the generated flows will propagate only over already-yielded sections.

The assigned hydraulic and strength parameters are reported in **Table 2**. They do not correspond to a specific site, but are rather chosen as typical literature values, very similar to those used by Salciarini *et al.* [51], by Schilirò *et al.* [53] or by Fusco *et al.* [21]. Once the material has reached instability, instant mobilization is assumed. The fluidized soil-water mixture is assumed to behave according to a Bingham model, with $\tau_0 = 700$ Pa and $\eta_B = 400$ Pa $\cdot$ s.

The results of the triggering and propagation analysis are illustrated on **Fig. 3b-d**. The triggering analysis confirms that the four slopes sections reach instability at different times, sequentially from

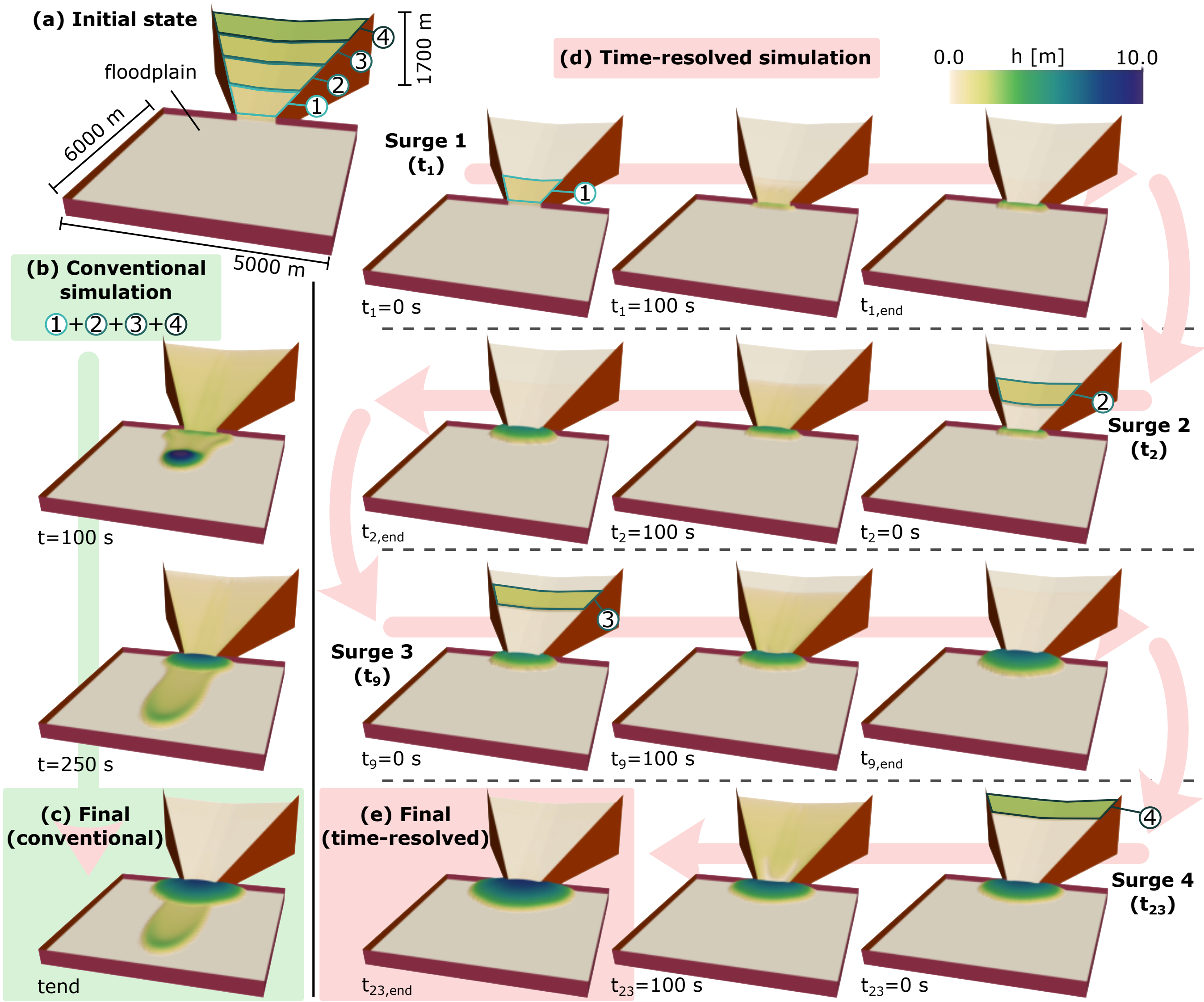

Fig. 3 (a) The adopted benchmark geometry, with highlight on the different slope sections that produce surges at different instants. (b) Runout simulation performed assuming an instantaneous instability of the whole slope, and (c) final configuration. (d) Runout simulation resolved in time, with surge tracking, and (e) final configuration after the last surge.

ϕ'	c'	γ_s	k	D
[°]	[Pa]	[kN/m^3]	[m/s]	[m^2/s]
18	2500	20	$2 \cdot 10^{-5}$	$5 \cdot 10^{-5}$

Table 2 Soil strength parameters for the benchmark slope. ϕ' is the friction angle, c' the cohesion, γ_s the soil specific weight, k_s the saturated hydraulic conductivity, D the saturated hydraulic diffusivity.

the steepest to the gentlest slope (1 to 4). In a conventional simulation (**b**), the collapse is assumed to occur instantaneously in all sections. The results of this simulation strategy are reported on the left column (green path). In this case, a significant portion of the unstable mass reaches the floodplain in a highly-dynamic state, and with sufficient inertia to spread almost 6000 m away from the fan apex, following the direction of the main slope. Over time, more material reaches the floodplain. However, this secondary flow does not possess sufficient inertia to spread over a long distance, leading to the accumulation of a deposit in the proximity of the fan apex (**c**). These results are consistent with the observations from laboratory tests [29].

The results of a triggering and runout with a time-resolved simulation (**d**) are illustrated on the right column (pink path). Here, the rainfall event is resolved with a sequence of 23 1-hour time intervals. A runout simulation is performed at the end of each interval. What is observed is that the steepest section (labelled as 1 in **Fig. 3a**) becomes unstable after only 1 hour of rainfall (t_1). This leads to the first surge, which mobilizes and propagates. The results of the runout analysis corresponding to this time interval are illustrated using three snapshots, respectively showing the surge height just after triggering ($t_1 = 0$ s), while propagating ($t_1 = 100$ s), and at its final state ($t_{1,\mathrm{end}}$). After the second rainfall interval t_2, a new instability concerning section 2 is triggered. The material mobilized by this instability is once more considered fully fluidized, and a new runout analysis is carried out. No further instability is recorded until the 9^{th} interval, when section 3 becomes unstable, and again at t_{23} when section 4 mobilizes, leading to the final deposit configuration (**e**).

Comparing the results of the time-resolved simulation (**e**) with the conventional one (**c**), a striking difference in the final deposit can be easily observed. This is due to widely different behaviour during runout. The time-resolved simulation leads to a sequence of flows with significantly lower inertia, and with shorter runout. Therefore, in this case, the conventional analysis grossly overestimates hazard at distance from the fan apex.

4 Description of the study cases

Two study cases are chosen for investigating how time resolution affects the back-analysis: the events of Sarno (1998) [10] and Giampilieri (2009) [19]. The cases are from the same geographical area, Southern Italy. They are characterized by extensive shallow instabilities leading to flow sequences with overlapping runout paths. Giampilieri and Sarno are relatively homogeneous with respect to the type of flows that were generated. They however differ in scale, with Giampilieri having a basin area about 10 times smaller. The relatively large amount of information available in the literature for both cases facilitates model calibration and validation.

4.1 Sarno event: May 5-6, 1998

Sarno is a small city in the Salerno province, Campania region, Italy. **Fig. 4** locates the area. The subsurface is characterized by the presence of pyroclastic deposits, originated from the explosive activity of the Vesuvius volcano [10].

On the 5^{th} and 6^{th} of May 1998, the region was hit by more than a hundred flow-like landslide events concentrated in the areas of Sarno, Quindici, Siano and Bracigliano (**Fig. 4a**). This caused widespread destruction, and around 160 casualties. The flows were triggered by prolonged rainfalls

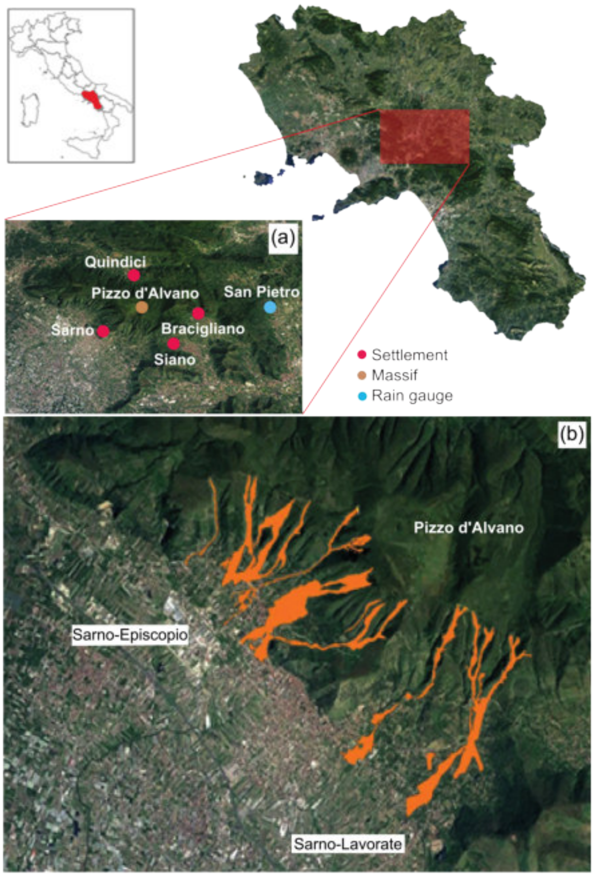

Fig. 4 (a) Sarno area location. (b) Flows path of the Sarno event of 5^{th} and 6^{th} of May 1998 (modified from Versace *et al.* [64]).

[14]: the event happened at the end of an exceptional rainy season, as appreciable by rainfall data of the months before [20]. Over the 48 hours when the slope instabilities occurred, the measured cumulative rainfall at the San Pietro monitoring station (**Fig. 4a**) reached 120 mm [11]. **Fig. 5** shows a detailed hyetograph of this event, with a 2-hour resolution. The rainfall event was not particularly intense. Nevertheless, a report by an environmentalist association argued that multiple factors contributed to increasing susceptibility, including a continuous series of wildfires during the years preceding the event [13]. The role of these predisposing factors has however not been fully confirmed in the scientific literature.

The pattern of flows that hit the Sarno area is shown in **Fig. 4b** [55]. As observable from the figure, shallow instabilities were widely distributed in the upper part of the slopes. The flows generated from the mobilization exhibited surges that reached the floodplain on various locations over 14 hours, flooding the outskirts of Sarno [13].

Field observation are available for performing a back-analysis. Specifically, **Fig. 6** reports the maximum flow heights as measured immediately after the event from the mud traces left on the buildings [50], in the Episcopio subsection (**Fig. 4b**). The figure also shows that the surge paths often overlap (i.e., multiple flows converged on the same area). However, no specific information is reported on the exact time-sequence of these events.

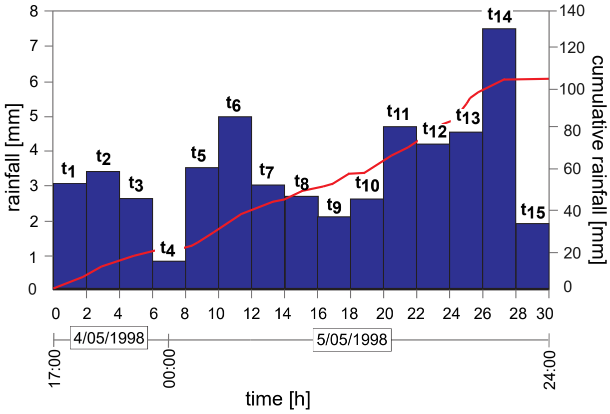

Fig. 5 Rainfall data of the 5th and 6th of May 1998, registered from the rainfall station at San Pietro [11]. In the hyetograph, fifteen rainfall-intensity intervals of two-hour duration are considered, named in the pictures with "t_i". The figure also shows the cumulated rainfall with a red continuous line.

Due to the dramatic consequences of the event, Sarno has been extensively back-analysed in the literature. Examples are the model by Sorbino *et al.* [55], and more recently by Fusco *et al.* [21]. An early runout analysis was presented by Revellino *et al.* [50] using a model analogous to RASH3D, but based on a pseudo-2D explicit Lagrangian solver [25].

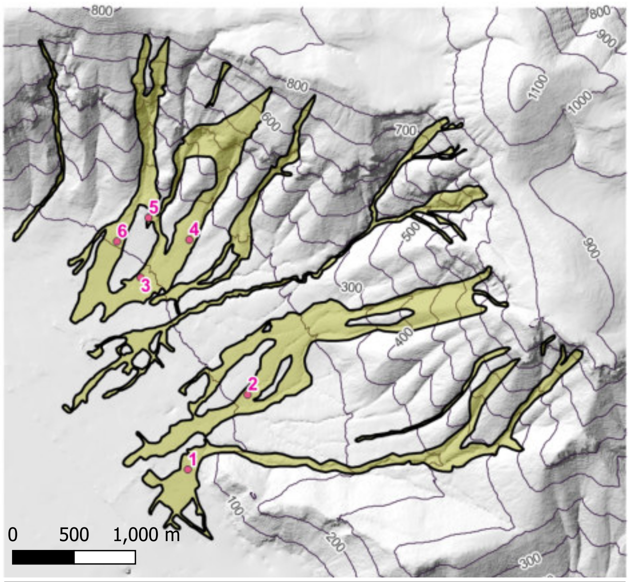

Point	1	2	3	4	5	6
h_{max} [m]	1.5-3.0	0.7-1.4	0.8-1.0	0.4-0.5	0.4-0.7	0.6-0.8

Observed impact area   Survey points

Fig. 6 Digital Elevation Model of Sarno - Episcopio (cell size: 5 x 5 m), with focus on measured maximum flow depths after the event [50].

4.2 Giampilieri event: October 1, 2009

Giampilieri is a small village, with less than two thousand inhabitants. **Fig. 7** shows its location in North-East Sicily, Italy. The village is surrounded by numerous steep slopes, from 30 to 60°, with an elevation from 50 to 400 m a.s.l., due to the presence of the Peloritani mountains. The slopes are mainly composed of highly erodible metamorphic material [56].

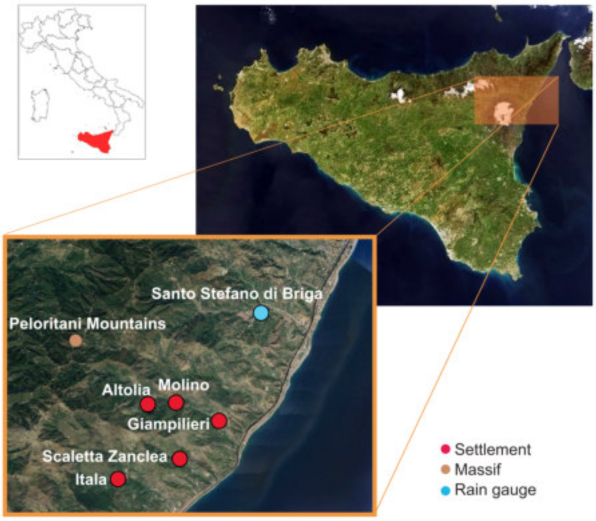

Fig. 7 Giampilieri area location.

On the 1st of October 2009 the Messina province was hit by a strong rainstorm, which caused around 600 shallow landslides in an area of 50 km^2. Consequently, causalities and damage to public and private properties occurred [19].

The area is characterized by a semi-arid climate. Nevertheless, the days prior to the event were characterized by continuous rainfall [58]. The preceding fifteen days saw the recoding of around 100 mm of cumulative rainfall at the monitoring station of Santo Stefano di Briga (highlighted on **Fig. 7**). **Fig. 8** shows the rainfall records on the day of the event, when a cumulative rainfall of almost 250 mm was reached in nine hours [58].

In **Fig. 9**, the Giampilieri runout path, along with the village buildings, is observable. The availability of this data is specified in Appendix A. Measured maximum flow depths at multiple location within the village, available from field observations, are reported in the inset on **Fig. 9** [58].

Triggering of the Giampilieri event has been already numerically back-analysed by Schilirò *et al.* [53] and by Stancanelli *et al.* [58] through a process-based method using TRIGRS. With regard to runout back-analyses, Stancanelli and Foti [56] proposed a comparison between two common approaches: a single-phase model [38], and a more sophisticated two-phase model [3]. A common trend in these reports is the difficulty in obtaining realistic values of flow heights, as confirmed also by La Porta *et al.* [30] using RASH3D. Bout *et al.* [7] applied the model OpenLISEM [18,17] to back-anaylse the event. The software simulates the sequence of shallow landslides, and their evolution into

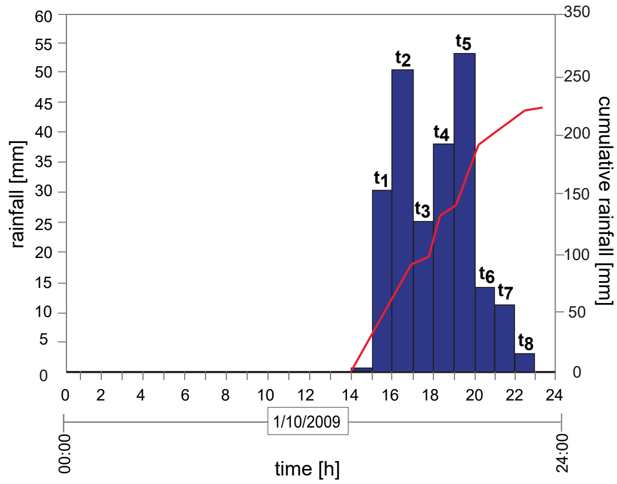

Fig. 8 Rainfall data, with 1-hour resolution, registered on the 1st of October 2009 at the rainfall monitoring station of Santo Stefano di Briga [58]. The station is the closest to Giampilieri. In the hyetograph, eight rainfall-intensity intervals of one-hour duration are considered, named in the pictures with "t_i". The figure also shows the cumulated rainfall with a red continuous line.

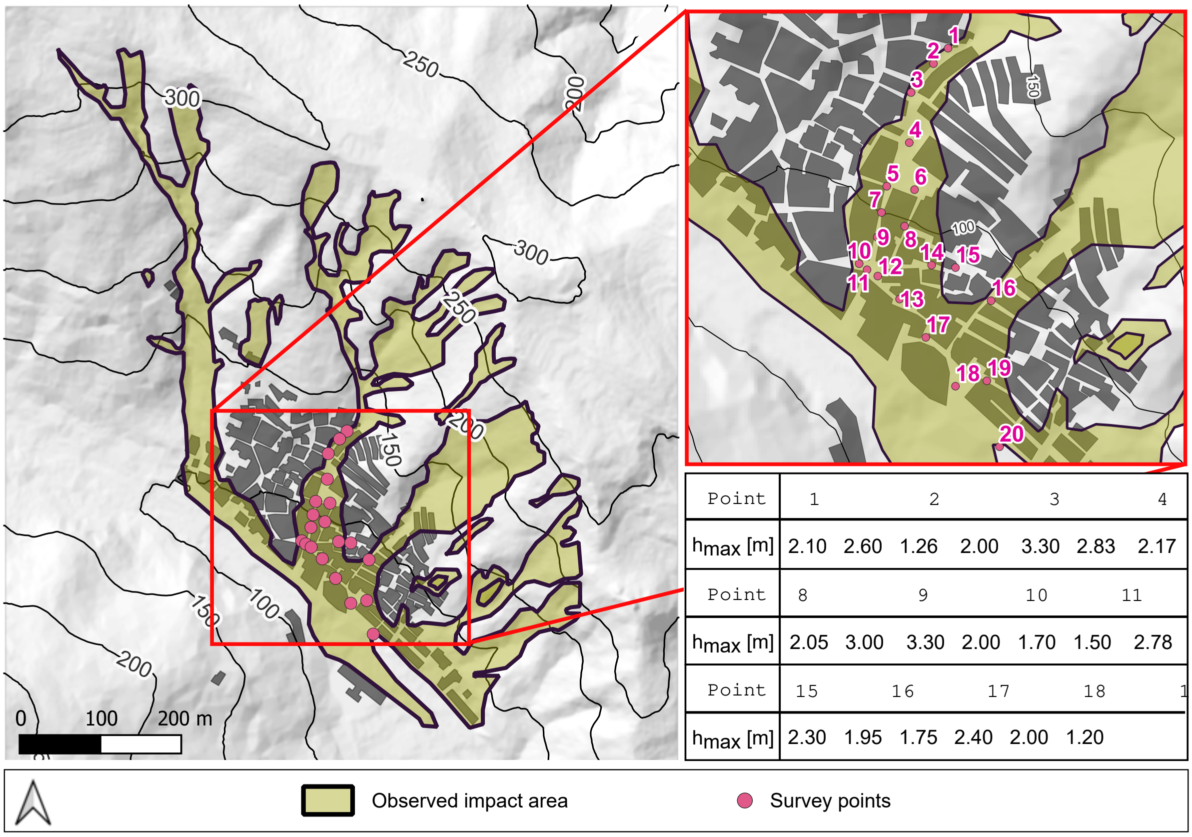

Fig. 9 Digital Elevation Model of Giampilieri (cell size: 2 × 2m), with focus on the 2009 event. The figure shows the flooded area during the event, and the buildings in the village. In the inset, the maximum flow depths on a sequence of surveyed points are reported, following Stancanelli *et al.* [58].

flows and flash floods, within a single numerical framework. The authors highlighted how multiple contributing factors need to be considered for achieving an accurate back-analysis (among others, the hydrology contribution to the flow runout simulation).

5 Analysis of obtained results

The goal of this section is applying the time-resolved procedure to the study cases. The results are compared with those obtained from conventional simulations set with the same input parameters.

5.1 Sarno event

The triggering analysis of the Sarno event is performed on the Episcopio subsection of the area (**Fig. 4b**). This area is adopted for the presence of multiple converging runout paths. The input parameters are chosen to be as consistent with the literature [55] as possible. **Table 3** lists the soil parameters used in the simulation. The distribution of permeable (i.e., mobilizable) soil depth d_l is taken from a publicly-available database (Appendix A), and is visualized in **Fig. 10**. The water table is considered at the analysis start as being coincident with the depth of permeable soil. The value of hydraulic conductivity k is calibrated to obtain a distribution of unstable cells that agrees with the findings of Sorbino *et al.* [55].

ϕ' [°]	c' [Pa]	γ_s [N/m^3]	k [m/s]	D [m^2/s]
38	5000	15000	$3 \cdot 10^{-5}$	$5.9 \cdot 10^{-5}$

Table 3 Soil parameters of the Sarno case study, used for the triggering analysis. The hydraulic conductivity is slightly increased with respect to previous back-analyses (from $1.0 \cdot 10^{-5}$ to $3.0 \cdot 10^{-5}$ m/s) to obtain a distribution of unstable areas consistent with Sorbino *et al.* [55].

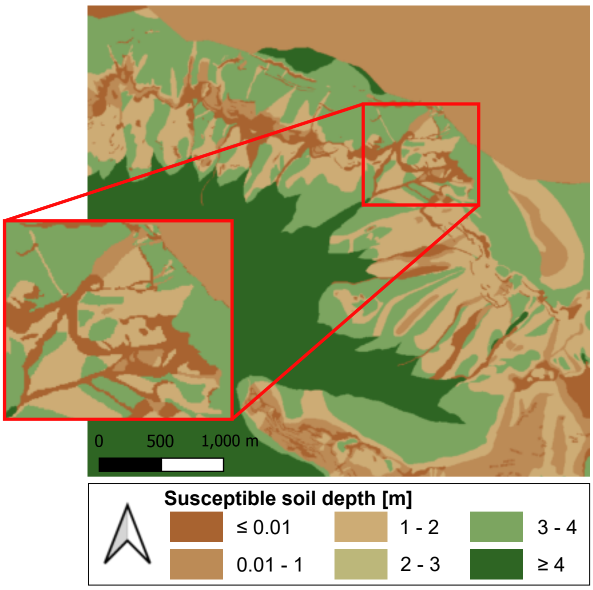

Fig. 10 Depth of permeable soil of the Sarno study area. Source specified in Appendix A.

The rainfall hyetograph used for the triggering analysis is reported in **Fig. 5**. As specified in Sec. 2, the hyetograph is provided with regular 2-hour intervals, and a constant average rainfall intensity for each interval is considered, uniform across the whole area. The triggering detection follows the same time resolution, and the results are reported in **Fig. 11a**. It is noticeable that at the end of the first time-interval, t_1, most of the triggering area already reached the instability threshold ($F_S \leq 1$). This aspect had not been investigated in earlier works, where the time-sequence of instabilities was not displayed [55,21]. The early mobilization of significant volumes is inconsistent with records from the day of the event, with observers reporting surges distributed over 12 hours [13]. However, in the conventional approach this inconsistency has no impact on the back-analysis, as all volumes are assumed to mobilize at the same time.

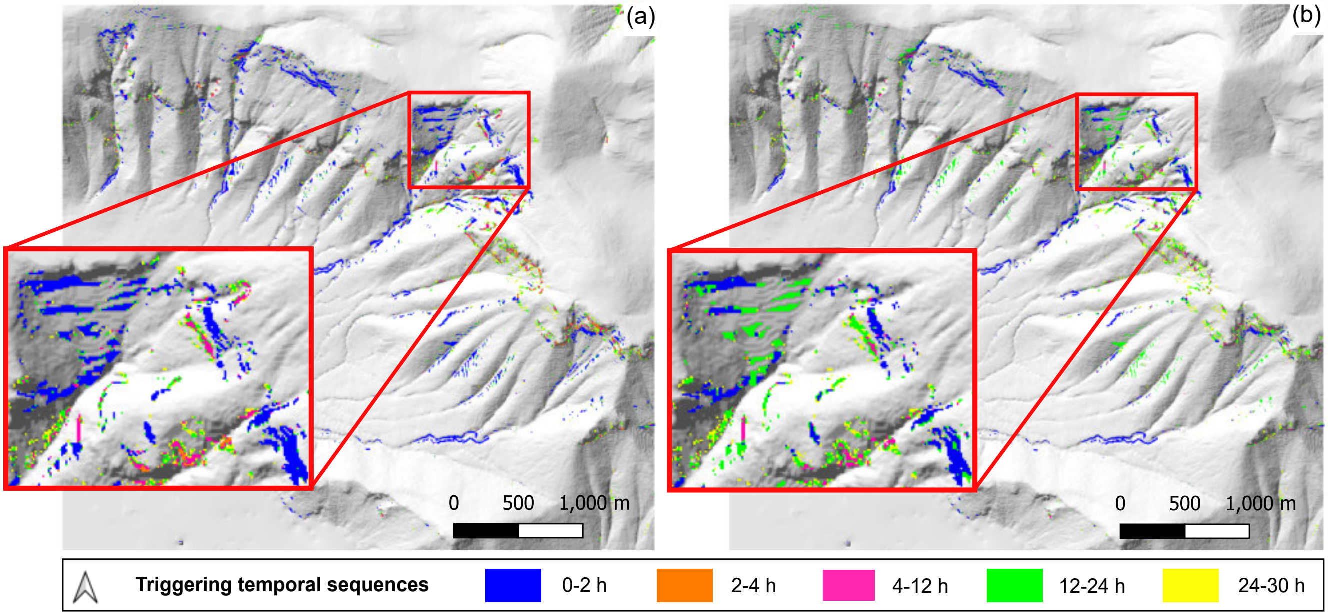

Fig. 11 Triggering analysis of the Sarno study case, with the instability sequence elaborated as a function of the input rainfall event. Panel (a) shows the results obtained using literature values, and panel (b) the results obtained hypothesizing a reduction of 20% in the depth of erodible soil.

The runout step is performed via a preliminary calibration of the rheology. The Bingham parameters are varied within intervals consistent with Pirulli *et al.* [45]. For τ_0 this is between 700 and 2000 Pa and for η_B between 300 and 500 Pa $\cdot$ s. The time-resolved and the conventional approaches lead to results that can be significantly different. Therefore, the rheology calibration procedure leads to different parameters when performed with the two approaches. This highlights how a back-analysis with a conventional approach might yield a biased set of calibrated parameters. In this work we aim at isolating time-dependency effects, and therefore we opt for showing the results obtained using the rheology calibrated on the time-resolving procedure. The same rheology is then used on the conventional approach for comparison. Validation is performed by comparing the values of maximum flow height recorded in the simulations with the surveyed flow heights, reported in **fig. 6** [50]. **Fig. 12** shows the best fit, which is obtained with $\tau_0 = 1000$ Pa and $\eta_B = 300$ Pa $\cdot$ s. In **Fig. 12a** the simulated maximum flow heights obtained with the conventional approach are displayed, overlaid on the contour of the surveyed flooded area. The conventional analysis captures well most of the surges.

However, on the floodplain runout is overestimated. This is probably due to the Bingham rheology being inadequate to describe the deposition phase, because it lacks a frictional component. Therefore, it is uncapable to simulate the re-mobilization of interparticle friction that occurs when excess pore pressures dissipates at deposition.

In **Fig. 12b**, the results obtained with the time-resolved procedure are shown. Herein, each unstable volume is mobilized at the instant in which instability occurs, as described in Sec. 2. To compare these results with those pertaining to the conventional approach, a contour of the maximum flow heights across all surges is presented. It is evident that there are no major differences in terms of maximum heights, or in the flooded area.

5.2 Giampilieri event

The Giampilieri study case was back-analysed employing the set of soil parameters proposed by Peres and Cancelliere [43] (**Table 4**). The thickness of the susceptible soil d_{l} is calculated using an empirical equation proposed by the same authors:

$$d_{\mathrm{l}} = 32exp(-0.07\delta) \tag{5}$$

which correlates locally the susceptible soil thickness with the main slope δ. The water table is initially considered to be coincident to the susceptible soil depth. In **Fig. 8**, the rainfall data used for the analysis are reported. Eight rainfall intervals are analysed, corresponding to the hourly variation of rainfall intensity. The first intensity is neglected, because its value (around 2 mm/h) is particularly low compared to the following ones.

ϕ' [°]	c' [Pa]	γ_{s} [N/m^3]	k [m/s]	D [m^2/s]
39	4000	19000	$2 \cdot 10^{-5}$	$5 \cdot 10^{-5}$

Table 4 Giampilieri, characteristics of the soil used for the triggering analysis [43].

Fig. 13 shows the distribution of unstable cells. The cells are grouped based on the time (from the rainfall event start) in which the instability condition $F_{\mathrm{S}} \leq 1$ is reached. The first two steps t_1 and t_2 do not exhibit any instability. Opposite to the Sarno study case, the instability process is here greatly spread over time, with triggering instabilities scattered over the whole rainfall event.

The runout model is calibrated varying the yield stress τ_0 between 500 and 1200 Pa and the plastic viscosity η_{B} between 100 and 1500 Pa $\cdot$ s. As for the Sarno study case, the conventional approach is compared to the time-resolved procedure. **Fig. 14** contains the best-fit simulation, in terms of runout path, which corresponds to $\tau_0 = 1000$ Pa and $\eta_{\mathrm{B}} = 1000$ Pa $\cdot$ s. The topography here features runout

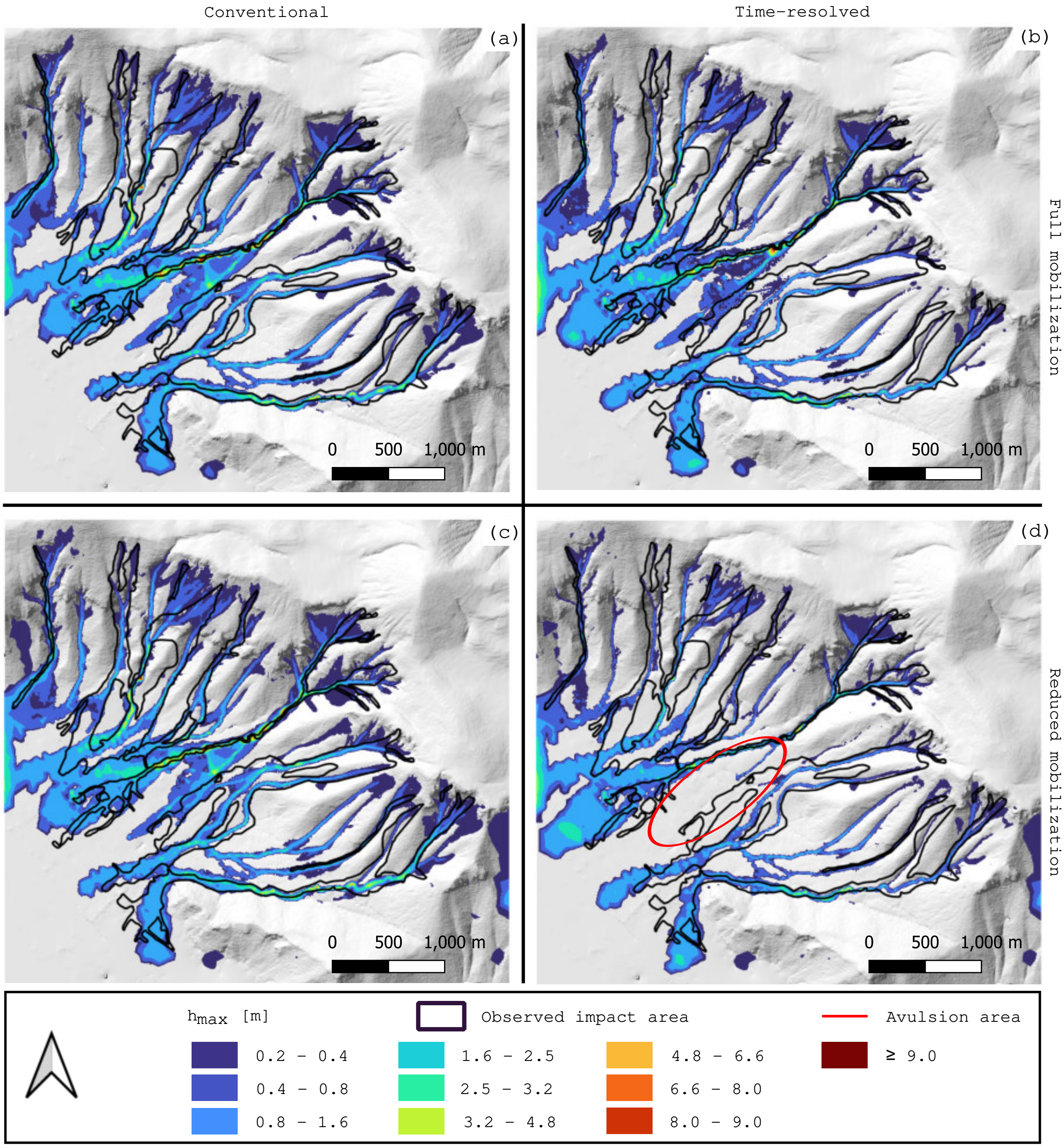

Fig. 12 Comparison between the conventional approach and the time-resolved procedure for the Sarno study case. Panels (a) and (b) show the conventional and the time-resolved simulation, respectively, performed assuming full mobilization of the erodible soil. Panels (c) and (d) compare the conventional approach and the time-resolved procedure, assuming a reduction of 20% in the depth of erodible soil d_l.

paths that merge and overlap within the settlement. For this reason, the settlement buildings were included in the digital elevation model, as local variations of the topographical coordinate.

In the Giampilieri study case, the comparison between the conventional approach and the time-resolved procedure (**Fig. 14**) shows significant differences, particularly appreciable in terms of runout path and flow path inside the settlement. This will be discussed in-depth in the next section.

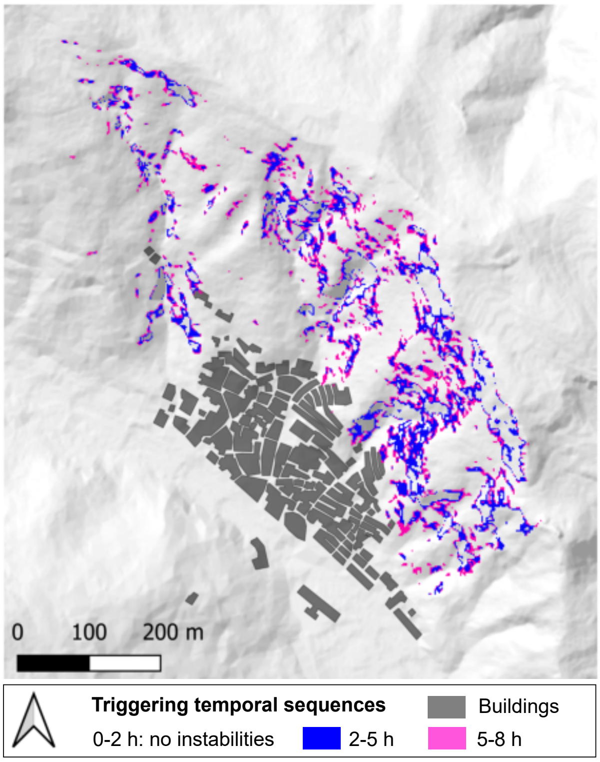

Fig. 13 Triggering analysis of the Giampilieri study case. Unstable cells are grouped depending on the time interval of first mobilization.

5.3 Comparison between conventional approach and time-resolved procedure

The comparison between the conventional approach and the time-resolved procedure reveals key aspects related to how events that occur over a long time period, such as the two selected study cases, develop.

The back-analysis of the Sarno study case featured numerous cells that de-stabilize in the initial detection time t_1. This detection time corresponds to the first two hours of the rainfall hyetograph. This time sequence is shown on **Fig. 11a**. After the initial release at t_1, there is no significant increment of unstable areas for the remaining considered instants $t_2 - t_{15}$. That is to say, most of the unstable mass is released during the first interval of the sequence. In this case, no significant differences between the two types of back-analysis are noticeable. In **Fig. 15a**, the maximum flow heights corresponding to the survey points highlighted on **Fig. 6** are displayed. Simulated and surveyed values are compared. The figure shows how the results are almost identical in the two approaches (light blue points for the conventional method, red points for the time-resolved procedure). This is appreciable in terms of maximum flow height over the whole back-analysis.

As mentioned already in Sec. 5.1, this highlights a problematic aspect, which is probably present in the previous attempts at back-analysing the event. The initial occurrence of numerous instabilities (t_1) is probably not realistic. In fact, in the real event the surges were observed from t_{11} onwards [13]. Even more worrying, the triggering analysis highlights that many cells are already unstable even at t_0, i.e. no rainfall is necessary to generate instability there. This makes it therefore apparent that the

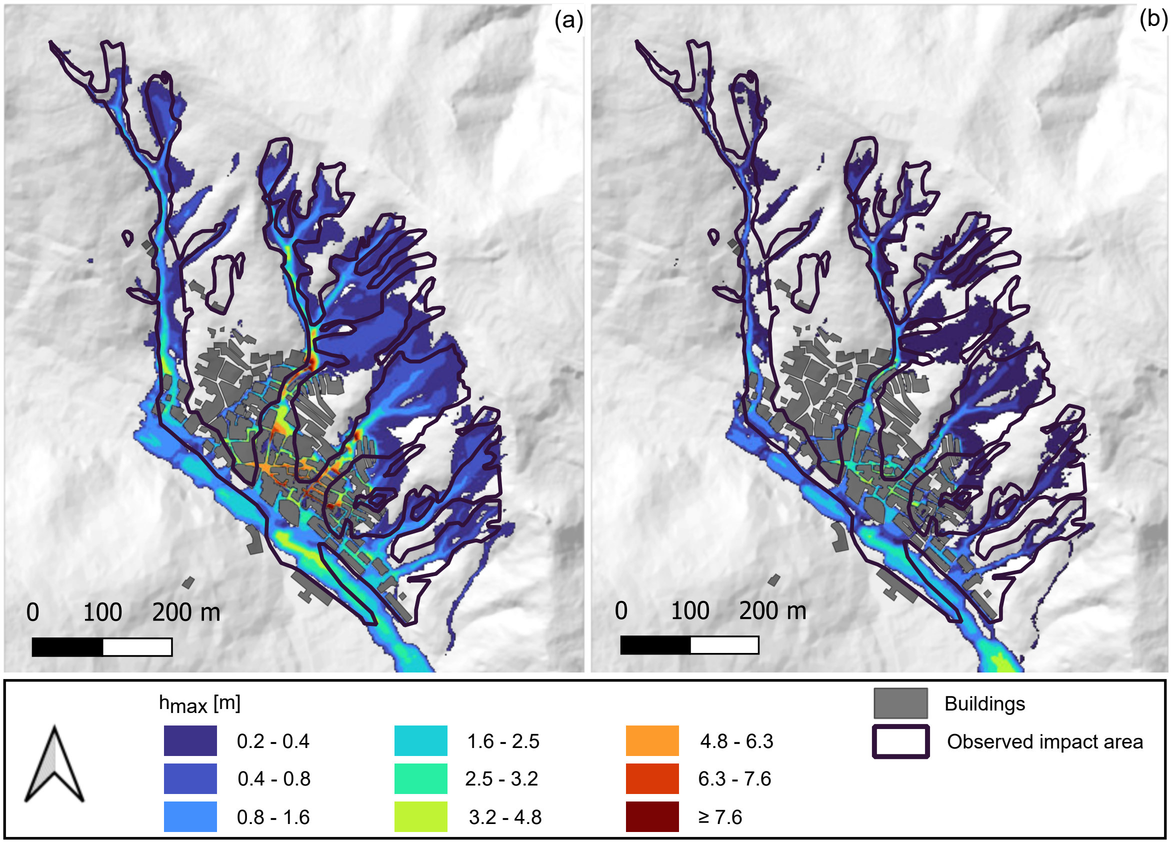

Fig. 14 Back analysis results for the Giampilieri study case. The contours show the value of maximum flow height for (a) the conventional approach and (b) the time-resolved procedure.

triggering parameters require further calibration. Nevertheless, the final results of the runout analysis appear accurate.

To understand the origin of this mismatch, some further analyses are performed. The susceptibility to instability is reduced by modifying the morphological parameters. In particular, the susceptible soil depth d_l is decreased. This leads to different results in the triggering analysis, which are shown in **Fig. 11b** for a reduction of 20% in d_l. From the distribution of unstable cells, it is evident that the instability process is now more widely distributed in time with respect to the original data (panel (**a**)). Nevertheless, this modification does not induce widely different results in the runout analysis. Comparing panels (**a**) and (**c**) in **Fig. 12**, reveals that the conventional approach with full mobilization or with reduced mobilization (d_l reduced by 20%) yields comparable results. Thus, the conventional approach appears relatively insensitive to a global reduction in susceptibility. However, when time-resolution is taken into account, the differences in results are much more pronounced (see panels (**b**) and (**d**)). In the reduced-mobilization analysis, instabilities are distributed in time over the whole event. Thus, the maximum flow heights recorded during runout are lower if the time-resolved procedure is adopted. Furthermore, distributing the surges more evenly over the event leads to the correction of a spurious avulsion phenomenon (highlighted in panel (**d**)).

Conversely, the Giampilieri study case shows an interesting sensitivity to the simulation method without altering the parameters. From the comparison between the conventional approach and the

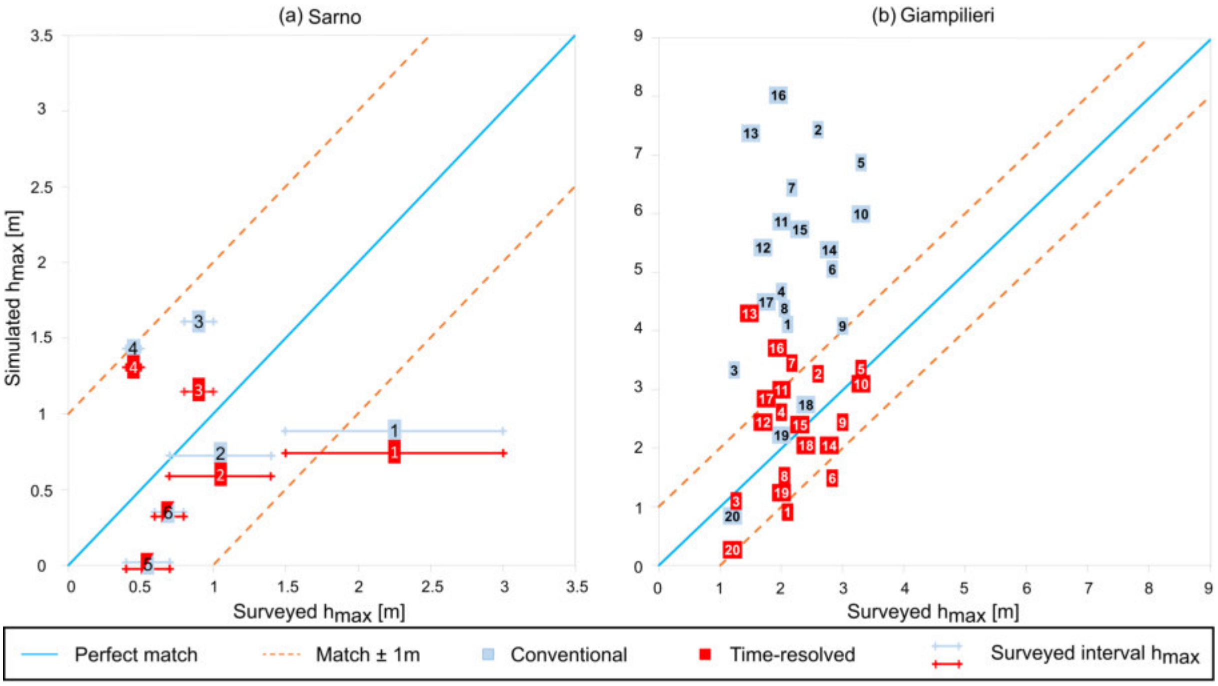

Fig. 15 Quantitative comparison of the performance of the conventional approach and of the time-resolved procedure on the two study cases. The graphs display the simulated maximum flow heights during the runout analysis with the two approaches, comparing simulated and surveyed values. The numerical labels correspond to the surveyed points whose location is described in **Fig. 6** and **Fig. 9**. The continuous blue line represents the perfect match with the surveyed flow heights. An acceptable error interval of ±1m is indicated with orange dashed lines.

time-resolved procedure (**Fig. 14**), two important differences can be observed. The variables of interest are the flow path and the maximum flow depths in the area inside the village, among the buildings. Here, with respect to the conventional approach, the time-resolved procedure yields a much more realistic runout, very similar to the surveyed one. This marked difference is also appreciable quantitatively. In **Fig. 15b**, the simulated maximum flow heights at the survey points of **Fig. 9**, are shown. The figure highlights how the two approaches yield significantly different results. Note that the simulation parameters are the same for the two simulations, as the only difference lies in the time resolution. The parameters are those consistent with the related literature. This means that the results for the conventional approach are already those corresponding to best-fit simulation. Nevertheless, the red points (time-resolved procedure) are much closer to the continuous blue line, which represents the perfect match with the survey values. Therefore, in this case, the time-resolved procedure simulates the event with higher accuracy. This is due to two reasons. Firstly, triggering analysis parameters available from Peres and Cancelliere [43] yield a realistic distribution of the instabilities, which reflect in a good performance of the time-resolved procedure in capturing the distribution of surges in time. Secondly, the Giampilieri study case is relatively small-scale. Therefore, minor topographical features, such as the buildings, are able to convey the flows on narrow channels (in this case, the village street). Thus, an incorrect representation of the surge sequence leads to much more evident errors in the back-analysis of flow heights.

6 Conclusions

Rainfall-induced shallow landslides often lead to soil mobilization, which in turn generates hazardous flows. These phenomena can be distributed over a wide area, with multiple instabilities generated by the same rainfall event. In this paper, a novel methodology for resolving the time and space sequences of mobilized shallow landslides of this type is proposed. In this new time-resolved procedure, triggering and runout are approached with different methods, applyed in a staggered fashion. Triggering is modelled through a simplified limit equilibrium method, suitable for the analysis of rainfall-induced shallow landslides. Runout is studied with a continuum numerical model, based on the solution of the depth-averaged equations for mass and momentum conservation, and with a Bingham rheological law.

The methodology is benchmarked on a simplified geometry, and then applied to back-analyse two sequences of shallow landslides and flows that occurred in Southern Italy. The analysis has highlighted that, even on a simplified geometry, the time-resolving procedure can lead to significantly different runout sequences. When the rainfall resolution is fine enough to separate in time the surges, spurious merging of mobilized material on the runout path is avoided, resulting in smaller and less momentous surges, with lower capacity to propagate on gentle inclines. The resolution in time appears to play a critical role when back-analysing event sequences with long duration. It leads to more realistic results, in terms of both flow path and maximum flow heights reached during the event. In the Giampilieri study case, which is characterized by multiple surges impacting a settlement, this has led to a much more accurate back-analysis of the event. To correctly apply the time-resolved procedure, it is important to have a resolution of rainfall that is fine enough to capture the events.

The proposed numerical procedure deliberately uses simplified tools for both triggering and runout. Thus, it has been shown that time-dependent effects can emerge without recurring to complex modelling. Nevertheless, future studies are clearly needed to remove some of the restrictions of the current procedure. In particular, the triggering model currently does not consider the mutual influence of adjacent cells. Phenomena such as retrogressive failure and wedging-ratcheting are ignored in the current formulation. A more accurate and realistic representation of the instabilities would also lead to a better representation of the runout, as was highlighted by the Sarno study case. Regarding the runout model, no bed erosion and entrainment has been considered in the study cases. Therefore, the triggering parameters might at present be under-estimated by back analysis, in order to compensate for the missing volumes mobilized by erosion.

Acknowledgements The authors acknowledge the financial support received from the MUR (Ministry of University and Research [Italy]) through the project "CLARA": CLoud plAtform and smart underground imaging for natural Risk Assessment (Project code: SCN_00451 CLARA/CUP J64GI4000070008), financed with the PON R&C 2007/2013 - Smart Cities and Communities and Social Innovation (National Research Program).

Appendix A. Obtaining maps of elevation and susceptible soil depth, and landslides event details for the two study cases

Digital Elevation Models were provided by the reference Regions (Sicily for the Giampilieri event, Campania for the Sarno one). The information of susceptible soil depth of the Sarno area (**Fig. 10**) can be downloaded from the following URL in shapefile format: *https://www.distrettoappenninomeridionale.it*. Italian landslide contours can be downloaded from the landslide inventory IFFI (Inventario dei Fenomeni Franosi in Italia), whose URL is: *https://www.progettoiffi.isprambiente.it*.

References

1. Aaron, J., McDougall, S., Moore, J. R., Coe, J. A., and Hungr, O. The role of initial coherence and path materials in the dynamics of three rock avalanche case histories. *Geoenvironmental Disasters 4*, 1 (2017), 5.
2. Anagnostopoulos, G. G., Fatichi, S., and Burlando, P. An advanced process-based distributed model for the investigation of rainfall-induced landslides: The effect of process representation and boundary conditions. *Water Resources Research 51*, 9 (2015), 7501–7523.
3. Armanini, A., Fraccarollo, L., and Rosatti, G. Two-dimensional simulation of debris flows in erodible channels. *Computers & Geosciences 35*, 5 (2009), 993–1006.
4. Barnhart, K. R., Jones, R. P., George, D. L., McArdell, B. W., Rengers, F. K., Staley, D. M., and Kean, J. W. Multi-Model Comparison of Computed Debris Flow Runout for the 9 January 2018 Montecito, California Post-Wildfire Event. *Journal of Geophysical Research: Earth Surface 126*, 12 (2021).
5. Baum, R. L., Savage, W. Z., and Godt, J. W. TRIGRS — A Fortran Program for Transient Rainfall Infiltration and Grid-Based Regional Slope-Stability Analysis, Version 2.0. *U.S. Geol. Surv. Open-File Rep.* ., 2008-1159 (2008), 75.
6. Berzi, D., Jenkins, J. T., and Larcher, M. Debris flows: Recent advances in experiments and modeling. *Advances in geophysics 52* (2010), 103–138.
7. Bout, B., Lombardo, L., van Westen, C. J., and Jetten, V. G. Integration of two-phase solid fluid equations in a catchment model for flashfloods, debris flows and shallow slope failures. *Environmental modelling & software 105* (2018), 1–16.
8. Cascini, L., Cuomo, S., and Della Sala, M. Spatial and temporal occurrence of rainfall-induced shallow landslides of flow type: A case of sarno-quindici, italy. *Geomorphology 126*, 1-2 (2011), 148–158.
9. Cascini, L., Cuomo, S., Di Mauro, A., Di Natale, M., Di Nocera, S., and Matano, F. Multidisciplinary analysis of combined flow-like mass movements in a catchment of southern italy. *Georisk: Assessment and Management of Risk for Engineered Systems and Geohazards 15*, 1 (2019), 41–58.
10. Cascini, L., Cuomo, S., and Guida, D. Typical source areas of May 1998 flow-like mass movements in the Campania region, Southern Italy. *Eng. Geol. 96*, 3-4 (2008), 107–125.
11. Cascini, L., Guida, D., and Sorbino, G. *Il Presidio Territoriale: una esperienza sul campo.* Rubbettino Editore, Catanzaro, 2005.
12. Chen, H., Zhang, L. M., Gao, L., Yuan, Q., Lu, T., Xiang, B., and Zhuang, W. Simulation of interactions among multiple debris flows. *Landslides 14*, 2 (2017), 595–615.
13. Chiavazzo, G., Colombo, L., and Minutolo, A. *Fango, il modello Sarno vent'anni dopo.* Legambiente, 2018.
14. Crosta, G. B., and Dal Negro, P. Observations and modelling of soil slip-debris flow initiation processes in pyroclastic deposits: the Sarno 1998 event. *Nat. Hazards Earth Syst. Sci. 3*, 1/2 (2003), 53–69.
15. Cruden, D., and Varnes, D. Landslide types and processes. chapter 3 in landslides: Investigation and mitigation. special report 247. washington, dc: National research council. *Transportation Research Board* (1996).

16. Cuomo, S. Modelling of flowslides and debris avalanches in natural and engineered slopes: a review. *Geoenvironmental Disasters 7* (2020), 1–25.

17. De Roo, A., Offermans, R., and Cremers, N. Lisem: A single-event, physically based hydrological and soil erosion model for drainage basins. ii: Sensitivity analysis, validation and application. *Hydrological processes 10*, 8 (1996), 1119–1126.

18. De Roo, A., Wesseling, C., and Ritsema, C. Lisem: a single-event physically based hydrological and soil erosion model for drainage basins. i: theory, input and output. *Hydrological processes 10*, 8 (1996), 1107–1117.

19. Foti, E., Faraci, C., Scandura, P., Cancelliere, A., La Rocca, C., Musumeci, R., Nicolosi, V., Peres, D., and Stancanelli, L. Da giampilieri a saponara: analisi delle cause scatenanti e delle cause predisponenti. *Atti Dei Convegni Lincei-Accademia Nazionale Dei Lincei 270* (2013), 45–64.

20. Frattini, P., Crosta, G. B., Fusi, N., and Dal Negro, P. Shallow landslides in pyroclastic soils: a distributed modelling approach for hazard assessment. *Engineering Geology 73*, 3-4 (2004), 277–295.

21. Fusco, F., Mirus, B. B., Baum, R. L., Calcaterra, D., and De Vita, P. Incorporating the Effects of Complex Soil Layering and Thickness Local Variability into Distributed Landslide Susceptibility Assessments. *Water 13*, 5 (2021), 713.

22. Godt, J. W., and Coe, J. A. Alpine debris flows triggered by a 28 july 1999 thunderstorm in the central front range, colorado. *Geomorphology 84*, 1-2 (2007), 80–97.

23. Guzzetti, F., Mondini, A. C., Cardinali, M., Fiorucci, F., Santangelo, M., and Chang, K.-T. Landslide inventory maps: New tools for an old problem. *Earth-Science Reviews 112*, 1-2 (2012), 42–66.

24. Hansen, A., Franks, C., Kirk, P., Brimicombe, A., and Tung, F. Application of gis to hazard assessment, with particular reference to landslides in hong kong. *Geographical information systems in assessing natural hazards* (1995), 273–298.

25. Hungr, O. A model for the runout analysis of rapid flow slides, debris flows, and avalanches. *Canadian geotechnical journal 623* (1995), 610–623.

26. Hungr, O., Evans, S., Bovis, M., and Hutchinson, J. A review of the classification of landslides of the flow type. *Environmental & Engineering Geoscience 7*, 3 (2001), 221–238.

27. Hutchinson, J. Morphological and geotechnical parameters of landslides in relation to geology and hydrogeology. In *Proc., Fifth international symposium on landslides, 1988* (1988), Lausanne, AA.

28. Iverson, R. M. Landslide triggering by rain infiltration. *Water Resour. Res. 36*, 7 (2000), 1897–1910.

29. Jing, L., Kwok, C. Y., Leung, Y. F., Zhang, Z., and Dai, L. Runout Scaling and Deposit Morphology of Rapid Mudflows. *Journal of Geophysical Research: Earth Surface 123*, 8 (2018), 2004–2023.

30. La Porta, G., Leonardi, A., Pirulli, M., Castelli, F., and Lentini, V. Rainfall-triggered debris flows: triggering-propagation modelling and application to an event in southern italy. In *IOP Conference Series: Earth and Environmental Science* (2021), vol. 833, IOP Publishing, p. 012106.

31. Leonardi, A., Pirulli, M., Barbero, M., Barpi, F., Borri-Brunetto, M., Pallara, O., Scavia, C., and Segor, V. Impact of Debris Flows on Filter Barriers: Analysis Based on Site Monitoring Data. *Environmental and Engineering Geoscience 27*, 2 (2021), 195–212.

32. Leonardi, A., Wittel, F. K., Mendoza, M., and Herrmann, H. J. Lattice-boltzmann method for geophysical plastic flows. In *Recent Advances in Modeling Landslides and Debris Flows*. Springer, 2015, pp. 131–140.

33. Liu, J., Li, Y., Su, P., and Cheng, Z. Magnitude–frequency relations in debris flow. *Environmental geology 55*, 6 (2008), 1345–1354.

34. Liu, J., Li, Y., Su, P., Cheng, Z., and Cui, P. Temporal variation of intermittent surges of debris flow. *Journal of Hydrology 365*, 3-4 (2009), 322–328.

35. Marin, R. J., and Velásquez, M. F. Influence of hydraulic properties on physically modelling slope stability and the definition of rainfall thresholds for shallow landslides. *Geomorphology 351* (2020), 106976.

36. McPhee, J. *The control of nature*. Noonday Press (New York), 1989.

37. Ng, C. W. W., Leonardi, A., Majeed, U., Pirulli, M., and Choi, C. E. A Physical and Numerical Investigation of Flow–Barrier Interaction for the Design of a Multiple-Barrier System. *Journal of Geotechnical and Geoenvironmental Engineering 149*, 1 (2023).

38. O'Brien, J. S. *Physical Processes, Rheology and Modeling of Mud Flows (Hyperconcentration, Sediment Flow).* PhD thesis, Colorado State University, 1986.

39. Park, D. W., Nikhil, N., and Lee, S. Landslide and debris flow susceptibility zonation using trigrs for the 2011 seoul landslide event. *Natural Hazards and Earth System Sciences 13*, 11 (2013), 2833–2849.

40. Pasqua, A., Leonardi, A., and Pirulli, M. Coupling depth-averaged and 3d numerical models for the simulation of granular flows. *Computers and Geotechnics 149* (2022), 104879.

41. Pastor, M., Quecedo, M., González, E., Herreros, M., Merodo, J. F., and Mira, P. Simple approximation to bottom friction for bingham fluid depth integrated models. *Journal of Hydraulic Engineering 130*, 2 (2004), 149–155.

42. Peng, C., Li, S., Wu, W., An, H., Chen, X., Ouyang, C., and Tang, H. On three-dimensional sph modelling of large-scale landslides. *Canadian Geotechnical Journal 59*, 1 (2022), 24–39.

43. Peres, D. J., and Cancelliere, A. Estimating return period of landslide triggering by Monte Carlo simulation. *J. Hydrol. 541* (2016), 256–271.

44. Pirulli, M. Morphology and substrate control on the dynamics of flowlike landslides. *Journal of geotechnical and geoenvironmental engineering 136*, 2 (2010), 376–388.

45. Pirulli, M., Barbero, M., Marchelli, M., and Scavia, C. The failure of the Stava Valley tailings dams (Northern Italy): numerical analysis of the flow dynamics and rheological properties. *Geoenvironmental Disasters 4*, 1 (2017).

46. Pirulli, M., Bristeau, M.-O., Mangeney, A., and Scavia, C. The effect of the earth pressure coefficients on the runout of granular material. *Environmental modelling & software 22*, 10 (2007), 1437–1454.

47. Pirulli, M., and Mangeney, A. Results of back-analysis of the propagation of rock avalanches as a function of the assumed rheology. *Rock Mechanics and Rock Engineering 41*, 1 (2008), 59–84.

48. Pirulli, M., and Pastor, M. Numerical study on the entrainment of bed material into rapid landslides. *Geotechnique 62*, 11 (2012), 959–972.

49. Reichenbach, P., Rossi, M., Malamud, B. D., Mihir, M., and Guzzetti, F. A review of statistically-based landslide susceptibility models. *Earth-science reviews 180* (2018), 60–91.

50. Revellino, P., Hungr, O., Guadagno, F. M., and Evans, S. G. Velocity and runout simulation of destructive debris flows and debris avalanches in pyroclastic deposits, campania region, italy. *Environmental Geology 45*, 3 (2004), 295–311.

51. Salciarini, D., Godt, J. W., Savage, W. Z., Conversini, P., Baum, R. L., and Michael, J. A. Modeling regional initiation of rainfall-induced shallow landslides in the eastern umbria region of central italy. *Landslides 3*, 3 (2006), 181–194.

52. Savage, S. B., and Hutter, K. The motion of a finite mass of granular material down a rough incline. *Journal of fluid mechanics 199* (1989), 177–215.

53. Schilirò, L., Esposito, C., and Scarascia Mugnozza, G. Evaluation of shallow landslide-triggering scenarios through a physically based approach: An example of application in the southern Messina area (northeastern Sicily, Italy). *Nat. Hazards Earth Syst. Sci. 15*, 9 (2015), 2091–2109.

54. Shen, W., Zhao, T., Zhao, J., Dai, F., and Zhou, G. G. Quantifying the impact of dry debris flow against a rigid barrier by dem analyses. *Engineering Geology 241* (2018), 86–96.

55. Sorbino, G., Sica, C., and Cascini, L. Susceptibility analysis of shallow landslides source areas using physically based models. *Nat. Hazards 53*, 2 (2010), 313–332.

56. Stancanelli, L. M., and Foti, E. A comparative assessment of two different debris flow propagation approaches - Blind simulations on a real debris flow event. *Nat. Hazards Earth Syst. Sci. 15*, 4 (2015), 735–746.

57. Stancanelli, L. M., Lanzoni, S., and Foti, E. Mutual interference of two debris flow deposits delivered in a downstream river reach. *Journal of Mountain Science 11*, 6 (2014), 1385–1395.

58. Stancanelli, L. M., Peres, D. J., Cancelliere, A., and Foti, E. A combined triggering-propagation modeling approach for the assessment of rainfall induced debris flow susceptibility. *J. Hydrol. 550* (2017), 130–143.

59. Stolz, A., and Huggel, C. Debris flows in the swiss national park: the influence of different flow models and varying dem grid size on modeling results. *Landslides 5*, 3 (2008), 311–319.

60. Tan, D.-Y., Yin, J.-H., Qin, J.-Q., Zhu, Z.-H., and Feng, W.-Q. Experimental study on impact and deposition behaviours of multiple surges of channelized debris flow on a flexible barrier. *Landslides 17*, 7 (2020), 1577–1589.

61. Taylor, D. W. *Fundamentals of soil mechanics*, vol. 66. LWW, 1948.

62. Van Westen, C. J., Castellanos, E., and Kuriakose, S. L. Spatial data for landslide susceptibility, hazard, and vulnerability assessment: An overview. *Engineering geology 102*, 3-4 (2008), 112–131.

63. Varnes, D. J. *Landslide hazard zonation: a review of principles and practice.* No. 3. United Nations, 1984.

64. Versace, P., Capparelli, G., and Picarelli, L. Landslide investigations and risk mitigation. the sarno case. In *Proceedings of 2007 International Forum on Landslide Disaster Management* (2007), vol. 1, pp. 509–533.

65. Yagi, H., Sato, G., Higaki, D., Yamamoto, M., and Yamasaki, T. Distribution and characteristics of landslides induced by the iwate–miyagi nairiku earthquake in 2008 in tohoku district, northeast japan. *Landslides 6*, 4 (2009), 335–344.